Journal of Applied Polymer Science

# Synthesis and Characterization of Clay/Polyaniline Nanofiber Hybrids

**Baoxiang Wang,[1,2] Yichao Yin,[1] Chenjie Liu,[1] Shoushan Yu,[1] Kezheng Chen[1]**
[1]College of Materials Science and Engineering, Qingdao University of Science and Technology, Qingdao 266042, China
[2]State Key Laboratory of Polymer Materials Engineering, Sichuan University, Chengdu 610065, China
Correspondence to: B. Wang (E-mail: bxwang@qust.edu.cn) or K. Chen (E-mail: kchen@qust.edu.cn)

**ABSTRACT:** A modified interfacial polymerization was used to prepare polyaniline (PANI) nanohybrids. The influence of the synthetic route, amounts of bentonite, and the surfactant on the structure, morphology, and optical properties of the as-synthesized nanocomposite were investigated. These materials were characterized by field emission scanning electron microscopy (SEM), transmission electron microscopy (TEM), X-ray diffraction, ultraviolet–visible spectroscopy, thermogravimetric analysis, and rheometer. The results show that PANI could be intercalated into the interlayer of the bentonite. The interlayer space increased from 1.25 to 1.486 nm. Then, the hexadecyl trimethyl ammonium bromide was used to modify the surface of bentonite, which was helpful in hybridizing with PANI for its hydrophobic properties. Both the intercalated and coating structure were found in the bentonite/PANI nanohybrid. The TEM and SEM images verified that the surface of the bentonite plate was coated by PANI nanofibers. In addition, for the study of the electroresponsive behavior, the composite was dispersed in silicone oil, and its electrorheological characteristics were examined via both an optical microscope and a rheometer equipped with a high-voltage power source. © 2012 Wiley Periodicals, Inc. J. Appl. Polym. Sci. 128: 1304–1312, 2013

**KEYWORDS:** nanoparticles; nanowires and nanocrystals; nanostructured polymers; properties and characterization; rheology

Received 19 June 2012; accepted 13 August 2012; published online 3 November 2012
**DOI: 10.1002/app.38472**

## INTRODUCTION

Many conductive polymers, such as polypyrrole (PPy), polymethylbenzene, polyphenylene sulfide, polythiophene, and polyaniline (PANI), were successively found in the last century. PANI is a unique conducting polymer among the family of conjugated polymers, and it possesses good electrical conductivity, environmental stability, optical activity, and unique chemical sensing and is made by a cheap and simple syntheses.[1] PANI has been considered the most promising conducting polymer in practical applications because of its structural diversity and lower cost, especially its unique proton acid-doping mechanism, reversible properties, and excellent electrical properties. However, its poor mechanical properties, indissolubility in common organic solvents, and bad rheological properties have seriously hampered its large-scale application in various fields because of its shortcomings in molding process.[2,3] In recent years, interest in research on conducting polymer nanostructures (i.e., nanorods, nanotubes, nanowires, and nanofibers) has increased because they combine the advantages of organic conductors with low-dimensional systems, good physicochemical properties, and potentially useful applications.[4–8] For example, in sensor applications, the greater sensitivity and faster time response of nanostructured PANIs are caused by their higher effective surface area and shorter penetration depth for target molecules compared to its conventional bulk counterpart. One-dimensional nanopolyaniline particles play an important part in the manufacturing of nanoscale interconnected and functional units, which are related to electronics, optoelectronics, electrochemistry, and electromechanical devices, and are different from the random PANI particles.[9–11] Further studies have suggested that the molecular structure of PANI nanotubes are more orderly and have a higher conductivity and that they could be used in the manufacturing of gas sensors. For example, PANI nanofibers with a high specific surface area can be used as sensing materials on hydrogen chloride and ammonia because of their high sensitivity and response speed. When structural directing molecules, such as surfactants to the chemical polymerization, were added to the synthesis system, PANI nanostructures could be obtained another way. The addition of organic dopants with surfactant functionalities, emulsions, or micelles led to tubes, fibers, or rodlike structures.[12–17]

Through unremitting efforts, it was discovered that PANI modification technology can overcome its shortcomings to improve the processing performance of PANI and to prepare multifunctional composite materials, which could be used widely in electrical conduction, metal corrosion, electromagnetic shielding, microwave absorption, photocatalysis, photovoltaic, sensing, and other fields. In particular, inorganic nanoparticles and

PANI bond through a synergetic effect and combine their physical and chemical properties at the nanometer scale. Consequently, the combination properties of products are better than those of all of the single components. Many preparation methods, such as template, seed polymerization, *in situ* polymerization, interfacial polymerization, intercalation polymerization, emulsion polymerization, blending, self-assembly, and electrochemical synthesis, have been used to synthesize PANI/inorganic nanocomposites.

Bentonite is an aluminum phyllosilicate, mostly composed of montmorillonite, in which the lamina maintains charge balance by the adsorption of $Na^+$, $K^+$, $Ca^{2+}$, $Mg^{2+}$, and other cations. These ions can conduct mass exchange with inorganic ions, organic molecules, and organic cations. The exchange reaction between organic cations and hydrated cations in bentonite lamina, that is, so-called hydrophobization on the hydrophilic surface of the bentonite. Consequently, it improves the wetting action between the mineral and polymer matrix to increase the compatibility. Recently, many layered materials with lamellar structures have attracted researchers' interest for the preparation of polymer/clay nanocomposites because of its remarkable properties.[18–22] Among previous materials, PANI has become a promising material for the commercial applications of conducting polymers because of its easy processing, environmental stability, and economic efficiency.[23]

In this study, we explored a facile modified interfacial polymerization method to synthesize the PANI/bentonite nanohybrids. By interfacial polymerization, the monomer and initiator existed in different phases, which ensured the successful synthesis of the PANI nanofibers. Furthermore, the PANI was processed via polymerization not only coating the surface of the bentonite but also intercalating into its layers. The structure and properties of the products were characterized and analyzed with X-ray diffraction (XRD), field emission scanning electron microscopy (SEM), thermogravimetric analysis (TGA), ultraviolet–visible (UV–vis) spectroscopy, and transmission electron microscopy (TEM).

## EXPERIMENTAL

### Materials

Aniline (99%, Laiyang Fine Chemical Factory, Laiyang, China) was distilled under reduced pressure. The other materials, including ammonium persulfate [APS; $(NH_4)_2S_2O_8$, 98%)], hexadecyl trimethyl ammonium bromide (CTAB), and HCl (35%) were used as received. A silicone oil (Tian Jin Bodi Chemical Co., Ltd., Tian Jin, China, dielectric constant = 2.72–2.78, viscosity of (Kinetic viscosity) $\gamma = 500$ mm$^2$/s, and specific density = 0.966–0.974 g/cm$^3$ at 25°C) was used as a suspending liquid because it was relatively nonpolar and nonconductive with a direct-current (dc) conductivity of the order of magnitude of $10^{-12}$ to $10^{-13}$ S/m.

### Synthesis of Electrorheological (ER) Particles

**Synthesis of the PANI/Bentonite Nanohybrid.** In a typical synthesis of the bentonite/PANI nanohybrid, different amounts of bentonite (0.4464 g, 0.2232 g, 0.1116 g) was added to 50 mL of 1*M* HCl, and the mixture was stirred for 24 h. Then, 4 mmol of APS was added to the previous liquid, and the mixture was stirred for 3 h. At the same time, 16 mmol of aniline (to ensure that the ratio of the aniline to APS was 4 : 1) was added to 50 mL of chloroform to form a transparent solution. After it was stirred for 3 h, the bentonite solution was carefully put in the chloroform solution (to ensure that the interface was not damaged). Without overnight stirring, the resulting dark green precipitate was collected. Then, the products were isolated by centrifugation, washed with deionized water, and dried at 80°C for 12 h. The three as-obtained PANI/bentonite nanocomposite samples were named S1 (0.4464 g of bentonite), S2 (0.2232 g of bentonite), and S3 (0.1116 g of bentonite).

**Synthesis of the PANI/Organoclay Nanohybrid.** In a typical synthesis of the PANI/organoclay nanocomposite, 0.4464 g of bentonite and the surfactant CTAB (0.15, 0.3, and 0.6 g, respectively) were added to 50 mL of 1*M* hydrochloric acid. After 24 h of stirring, the precipitates were washed several times by deionized water to remove the dissociated CTAB. Then, the modified bentonite was redispersed into 50 mL of 1*M* hydrochloric acid, and the mixture was stirred for 24 h. Then, 4 mmol of APS was added, and this mixture was stirred for 3 h. At the same time, 16 mmol of aniline (to ensure that the ratio of aniline to APS was 4 : 1) was added to 50 mL of chloroform to form a transparent solution. After it was stirred for 3 h, the bentonite solution was carefully placed in the chloroform solution (to ensure that the interface was not damaged). Without overnight stirring, the resulting dark green precipitate was collected. Then, the products were isolated by centrifugation, washed with deionized water, and dried at 80°C for 12 h. According to the different amounts of as-used CTAB, the products were named S4 (0.6 g of CTAB), S5 (0.3 g of CTAB), and S6 (0.15 g of CTAB). During the hydrophobic treatment, the organoclay precipitate was centrifuged after the intercalated reaction and was washed several times with distilled water to ensure that no dissociated CTAB was detected in the next reaction system.

**Synthesis of the PANI/Organoclay Nanohybrids with Free CTAB.** The PANI/bentonite hybrids were synthesized, whereas free surfactant CTAB was always in the system. In a typical synthesis, 0.4464 g of bentonite and surfactant CTAB (0.15 g, 0.3 g, 0.6 g) were added to 50 mL of 1*M* hydrochloric acid, respectively. After 24 h of stirring, 4 mmol of APS was added to the modified bentonite, and the mixture was stirred for 3 h. At the same time, 16 mmol of aniline (to ensure that the ratio of aniline to APS was 4 : 1) was added to 50 mL of chloroform to form a transparent solution. After 3 h of stirring, the CTAB-modified bentonite solution was carefully placed in the chloroform solution. Without overnight stirring, the resulting dark green precipitate was collected. Then, the products were isolated by centrifugation, washed with deionized water, and dried at 80°C for 12 h. The PANI/bentonite nanohybrids were called S7 (0.15 g of CTAB), S8 (0.3 g of CTAB), and S9 (0.6 g of CTAB).

### Preparation of the ER Suspensions

ER suspensions of the PANI/bentonite nanohybrids in silicone oil were prepared with the following steps. Before the preparation of electrorheological fluid (ERF), the as-obtained S4 sample

Applied Polymer SCIENCE

was further immersed in an aqueous $NH_3$ solution overnight. The purpose of this treatment was to control the conductivity to a suitable range; this was helpful for the ER application. Finally, we obtained PANI/bentonite nanohybrid particles for the ERFs by filtering, drying, and milling. The obtained PANI/bentonite nanohybrids were desiccated in a vacuum oven at 80°C for 12 h (the degree of vacuum was 0.05 MPa.) and then mixed with silicone oil to form the ERF (20 wt %).

### Characterization

The crystal structure was determined by the powder XRD patterns (Rigaku D-max-$\gamma$A X-ray diffractometer, Rigaku Corporation,Tokyo, Japan) with Cu K$\alpha$ irradiation ($\lambda$ = 1.54178 Å). The morphology of the particles was observed by SEM (JEOL JSM-6700F, JEOL Ltd.,Tokyo, Japan) and TEM (JEOL JEM-2100F, JEOL Ltd., Tokyo, Japan). UV–vis spectra were taken on Varian Cary 500 UV–vis–near infrared spectrophotometer (Varian, Inc.,New Orleans, USA). To analyze the thermal stability and mass percentage of the samples, a thermogravimetric analyzer (STA449c TGA instrument, Netzsch-Ger Tebau GmbH, Selb, Germany) was used with a heating rate of 10°C/min from room temperature to 800°C. To measure the conductivity of the PANI/bentonite nanohybrids, dry samples were pelletized at 1100 MPa, and the electrical conductivity was measured with a resistivity meter (FZ-2010, Shang Hai Chang Bao Co., Ltd., Shang Hai, China) at room temperature. The conductivities of the PANI/bentonite nanohybrids before and after $NH_3$ treatment were 8.22 $\times$ $10^{-2}$ and 4.9$\times$ $10^{-8}$ S/cm, respectively.

A modified rotary viscometer (NXS-11A; Chengdu Instrument Factory, ChengDu, China) and a high-voltage dc power source (DPS-100; Dalian Dingsheng Technology Co.,Ltd., Da Lian, China.) were used to research the rheological properties of the ERFs. The ERF was placed into the gap between the stationary cup and the rotating bob. An applied mechanical torque sheared the ERF until the particle chains structures were broken so that the ERF could flow between the cup and the bob. Thereby, the shear rate was observed when the ERF started to flow. We initially applied the electric field on the suspension for 300 s and then sheared it to get the rheological data under the external electric field.

## RESULTS AND DISCUSSION

### Phase and Morphology Analysis

The principle of interfacial polymerization of the PANI nanofibers explains that a small amount of product appears in the first stage of traditional chemical oxidative polymerization. Subsequently, the reactive nanofibers, by a large number of monomer and oxidant, promote the radical polymerization to rapidly obtain some irregular PANI products. Because the monomer and initiator exist in different phases, the reaction only occurs in the oil–water boundary. However, the active PANI chains do not grow into the irregular particles because of the limited monomer around them. Subsequently, the reaction was inhibited when the particles separated from the interface into the aqueous solution and ensured that the resulting products were uniform in diameter nanofibers. The green PANI began to appear in the interface and ultimately spread to the entire aqueous phase with time.

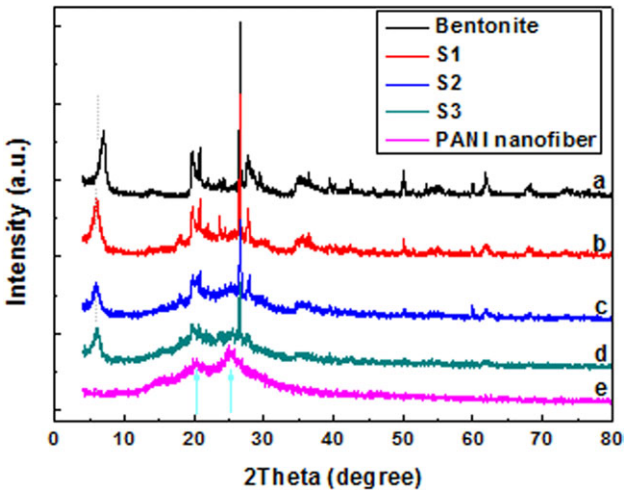


**Figure 1.** XRD patterns of the different PANI/bentonite nanocomposites, pure bentonite, and pure PANI nanofibers: (a) pure bentonite, (b) S1, (c) S2, (d) S3, and (e) pure PANI nanofibers. [Color figure can be viewed in the online issue, which is available at wileyonlinelibrary.com.]

The crystal structures of the samples were determined by XRD patterns. The pure PANI nanofibers had two relatively broad peaks at 20 and 25°, respectively, as shown in Figure 1(e). This suggested that the PANI was partial crystalline. In further study of the crystal structure of pure bentonite, the (001) characteristic diffraction peak appeared at $2\theta$ = 7.02°, so the spacing of the lamellar structure was 1.25 nm. Compared with pure bentonite, the diffraction patterns of the PANI–bentonite nanocomposites [S1, S2, and S3, Figure 1(b-d), obtained from process 1] showed a shift of the basal peak position from 1.25 to 1.486 nm ($2\theta$ = 5.98°). The increase in the *d*-spacing could be attributed to the intercalation of the polymers in the PANI/bentonite nanocomposites. In addition, the intensity of intercalated peaks was enhanced with increasing content of the bentonite, and the intensity of the PANI peaks was reduced simultaneously.

The binding ability increased when the bentonite was first treated by quaternary ammonium surfactant (CTAB) and hybridized with PANI. There were two paths for hydrophobic treatment in this research; one was that the surfactant was always present in the reaction system (see process 3), and the other was that the organoclay precipitate was centrifuged after the intercalated reaction and was washed several times with distilled water to ensure that no dissociated CTAB was detected in the next reaction system (see process 2). The XRD patterns [Figure 2(b–d)] of the as-obtained products with the second method had an obviously sharper diffraction peak at $2\theta$ = 5.98°; this reflected the strong influence of the hydrophobic treatment. Compared with the direct PANI/bentonite hybrid, the intercalation peaks increased further.

Further study of the XRD patterns [Figure 2(e–g)] of the products synthesized with process 3 showed a characteristic diffraction peak at $2\theta$ = 4.96° ($d_{001}$ = 1.78 nm), which expanded about 0.53 nm because of the intercalation of CTAB compared with pure bentonite, especially at high concentrations (S9: 0.6 g of CTAB) of surfactant. The intercalation peak of CTAB at $2\theta$

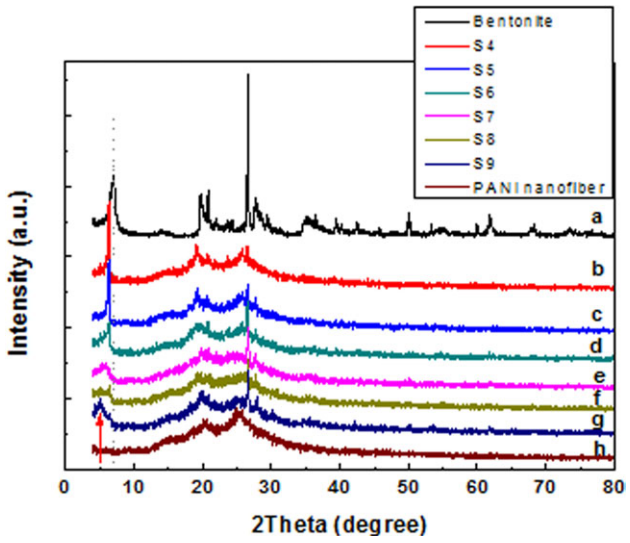


**Figure 2.** XRD patterns of the different PANI/organoclay nanocomposites modified by CTAB: (a) pure bentonite, (b) S4, (c) S5, (d) S6, (e) S7, (f) S8, (g) S9, and (h) pure PANI nanofibers. [Color figure can be viewed in the online issue, which is available at wileyonlinelibrary.com.]

$= 4.96°$ increased with increasing surfactant; at the same time, the PANI peak at $2\theta = 5.98°$ ($d_{001} = 1.486$ nm) became low. In the interfacial polymerization process, the CTAB free in the system influenced the formation of the stable and clear interface between water and oil (organic phase). The 001 diffraction peaks of the products were complex and included the intercalated peaks of PANI and the surfactant. Also, the surfactant free in the system stunted the formation of the PANI nanofibers.

SEM and TEM techniques were employed to examine the detailed morphology of the as-synthesized PANI/bentonite nanocomposites. The SEM photos of pure bentonite [Figure 3(a,b)] showed the presence of irregular granular aggregates; this reflected its layered nature with minute high-density granules per unit area. The size of bentonite was inhomogeneous, such as from several hundred nanometers to micrometers. So its distribution was polydispersed. Figure 3(c,d) shows the SEM images of the as-prepared PANI nanofibers via interfacial polymerization, which was displayed as fibers with a diameter of 30–60 nm and a length of 200–300 nm. SEM images revealed that they were actually agglomerations of nanofibers. The SEM images of the PANI/bentonite nanocomposites [Figure 3(e–h)] showed that the PANI fibers were incumbent on the surface of bentonite. The doped PANI possessed cations that were helpful in binding with clay, not only to form intercalation structures but also to coat onto the surface of bentonite.

TEM observation showed that the as-prepared S4 PANI/bentonite nanocomposites (Figure 4) obtained by method 2 were capped on the surface of the bentonite, which was previously confirmed by SEM. The TEM images demonstrated a fine nanofibrous structure of PANI on the surface of bentonite obtained with the modified interfacial polymerization process. The nanofibers had an average diameter ranging from 30 to 60 nm with characteristic lengths of 200–300 nm.

### TGA

TGA was performed on the PANI nanofibers, pure bentonite, and PANI/bentonite nanocomposite to determine their thermal stabilities under a nitrogen atmosphere. The TGA curves are given in Figure 5, where the initial weight loss up to 150°C for each curve was ascribed to the removal of water molecules. In the measured temperature range, the weight loss of the PANI/bentonite nanocomposite was lower than that of the pure PANI nanofibers. The increased thermal stability of the PANI/bentonite nanocomposite could have been due to the existence of inorganic bentonite nanolayers. The final weight loss of the PANI nanofibers was about 40%; this was bigger than that of the PANI/bentonite nanocomposite (S4 15.89%). The enhanced thermostability was also observed in S9 and was attributed to the thermostable clay particles, but the residual mass implied a lower amount of clay than in S4.

### UV–Vis Analysis

The UV–vis spectra of pure PANI nanofibers [Figure 6(a)] presented three peaks at 340, 440, and 800 nm; these corresponded to the oxidation state of the doped PANI. The first absorption band arose from the $\pi$–$\pi^*$ transition. The second and third bonds were related to the polaron band $\pi$–$\pi^*$ transition and the $\pi$ to the localized polaron band of doped PANI.[22,23] Characteristic absorption bands at wavelengths of 330–360, 420–440, and 790–820 nm were also observed in the curves of the PANI/bentonite nanohybrids at the same position. However, the spectrum intensity of the serial PANI/bentonite nanohybrids [Figure 6(b,c), obtained from process 1] decreased rapidly with the enhanced concentration of bentonite. Furthermore, the UV–vis diffuse reflectance spectra of the PANI/bentonite nanohybrids [Figure 6(d–f), obtained from process 2] after hydrophobic treatment by the surfactant CTAB indicated that the emission peaks were redshifted from 440 to 460 nm and were blueshifted from 340 to 300 nm. This confirmed that the hydrophobic treatment process promoted the binding ability between bentonite and PANI.

### ER Observation and Rheological Behavior

ERFs are a kind of smart materials consisting of suspensions of dielectric particles dispersed in a nonconducting liquid.[24–27] ERFs can exhibit drastic changes in their rheological properties, including large enhancements in the apparent viscosity, shear stress, modulus, and yield stress under an alternating-current/dc electric field.[28–30] The polarization of the suspended particles is induced by the application of an electric field, and a chainlike structure can be formed along the electric field direction in a few milliseconds.[30–35] Before the preparation of ERFs, the as-obtained S4 sample was further immersed in an aqueous $NH_3$ solution for several hours. Finally, we obtained the PANI/bentonite nanohybrid particles for the ERFs by filtering, drying, and milling. The S4 PANI/bentonite nanocomposite based ERF was prepared by the dispersal of the particles in silicone oil. Suitable conductivity plays as an important role in the high-ER effect because the high conductivity of ER materials can lead to a large leaking current density, and breakdown can occur under the high electric field. Meanwhile, the low conductivity leads to low-conductivity mismatch and the weak polarization of particles, so the ER effect is also weak. We also measured the ER

Applied Polymer SCIENCE

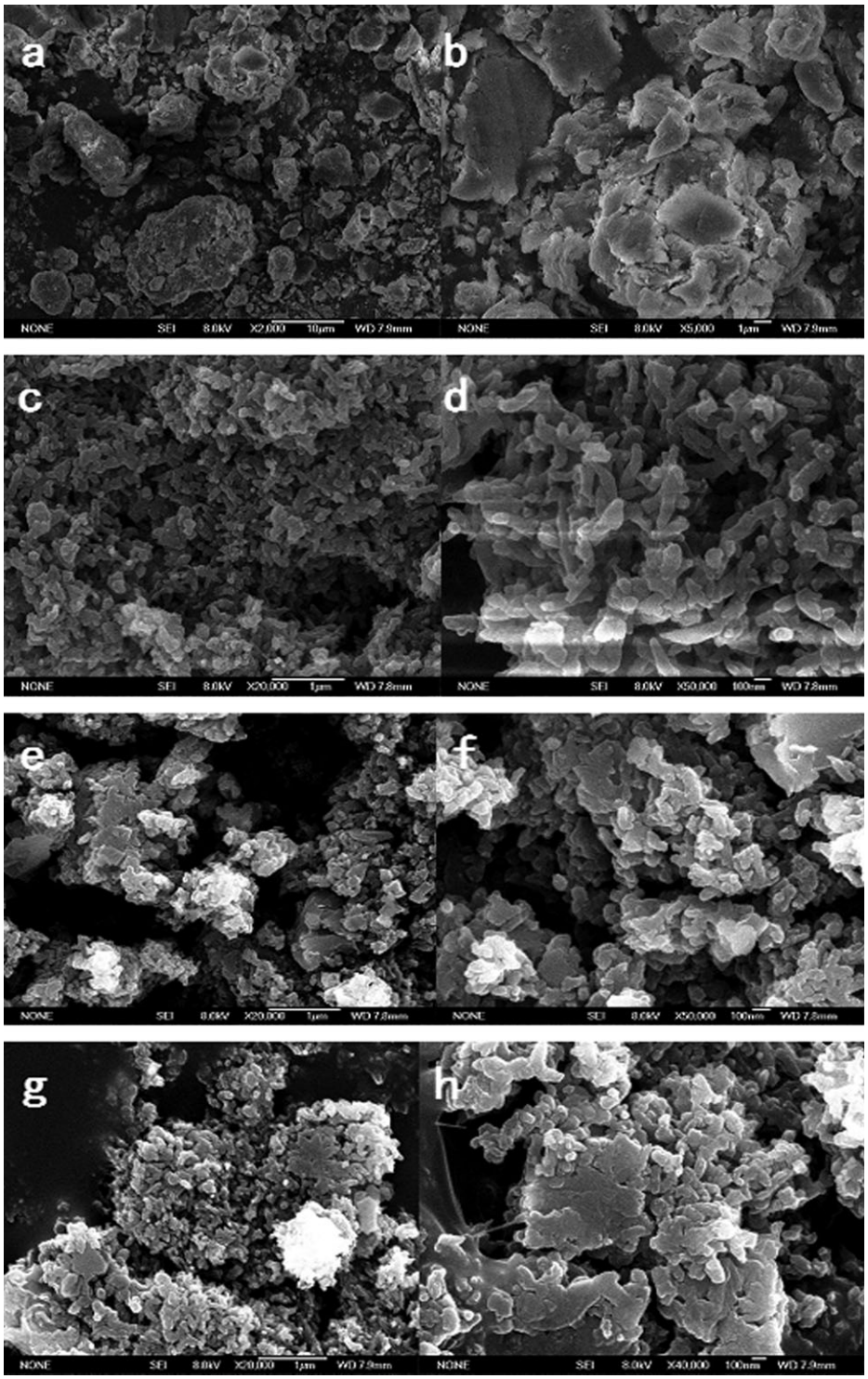


**Figure 3.** SEM images of different samples: (a,b) pure bentonite, (c,d) pure PANI nanofibers, (e,f) S1, and (g,h) S4.

behavior of the S4 sample without $NH_3$ treatment; however, the electric breakdown occurred even at $E = 1$ kV/mm, and it could not be used for the ERFs. To use the particles for an ERF, the electrical conductivity of the obtained S4 sample were controlled by a dedoping process in which an $NH_3$ solution was used. The conductivity was found to decrease from $8.22 \times 10^{-2}$ to $4.9 \times 10^{-8}$ S/cm via a dedoping process.

Similar dedoping processes also were also seen in other groups' work. The electrical conductivity of the obtained electrical conductivities of both PPy and PPy/organically modified montmorillonite nanocomposites were measured to be $4.5 \times 10^{-2}$ and $2.0 \times 10^{-3}$ S/cm, respectively. The conductivity of the PPy/organically modified montmorillonite nanocomposite was then controlled to be semiconducting ($1.1 \times 10^{-8}$ S/cm) via

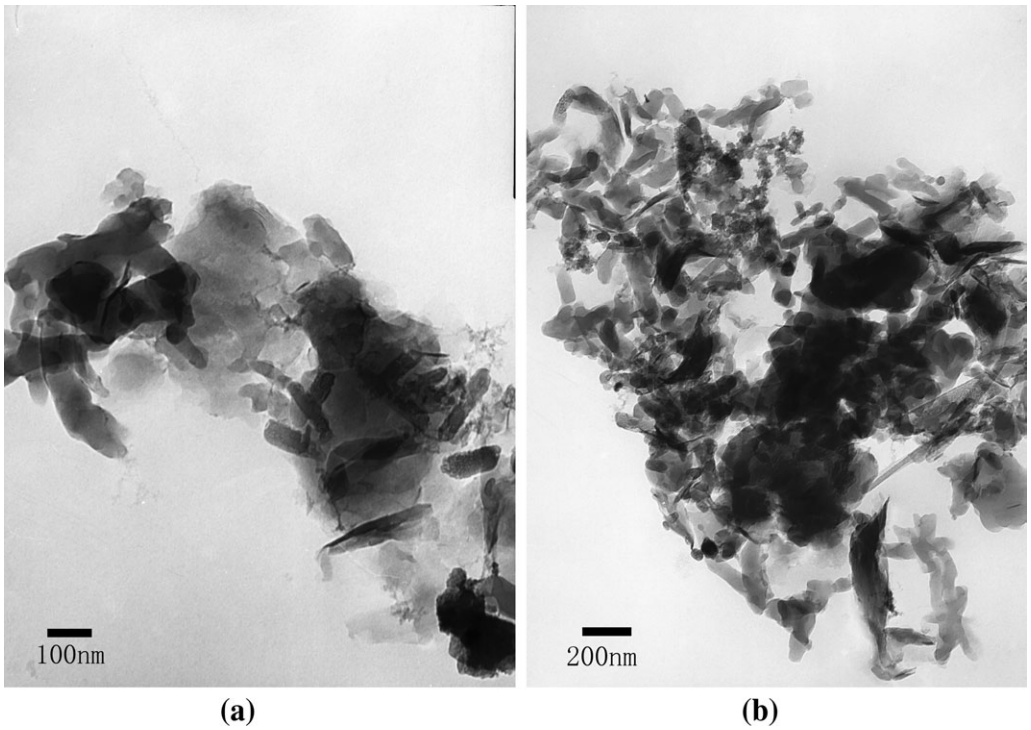


**Figure 4.** TEM images of the S4 PANI/organobentonite nanocomposites.

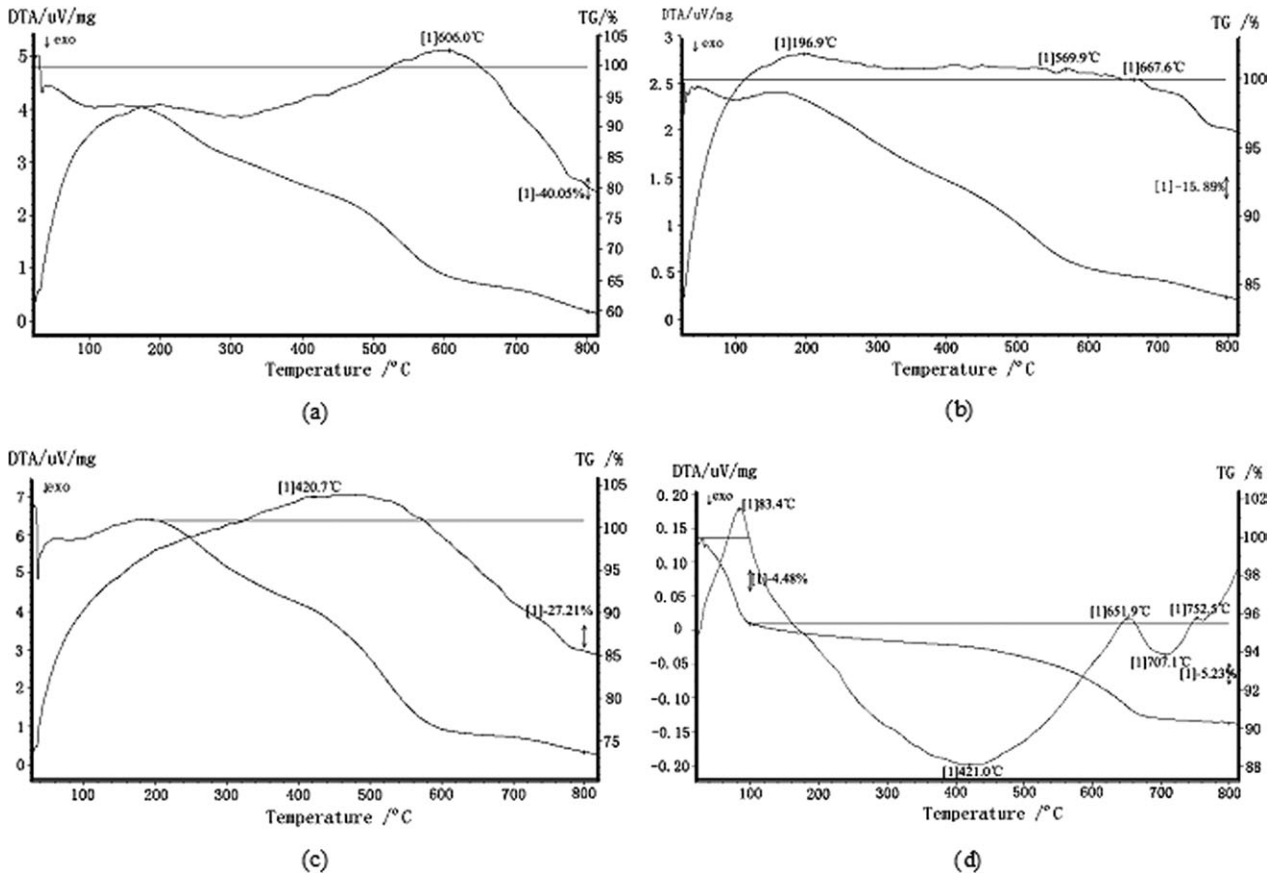


**Figure 5.** Thermogravimetry (TG)–differential thermal analysis (DTA) curves of the as-synthesized samples: (a) pure PANI nanofibers, (b) S4, (c) S9, and (d) pure bentonite.

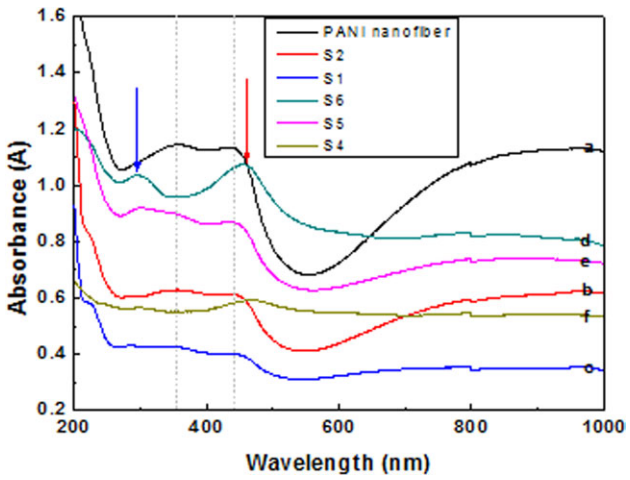


**Figure 6.** UV–vis spectra of the different samples: (a) pure PANI nanofibers, (b) S2, (c) S3, (d) S6, (e) S5, and (f) S4. [Color figure can be viewed in the online issue, which is available at wileyonlinelibrary.com.]

dedoping with NaOH for the ER application.[35,36] In another example, the conductivity of kaolinite/dimethyl sulfoxide/carboxymethyl starch ternary nanocomposites was adjusted to an optimum point ($10^{-6}$ to $10^{-8}$ S/cm) that was beneficial to ER activity via a change in the component ratio of ternary nanocomposites.[37] In addition, Block et al.[38] reported that ERFs with a conductivity of around $10^{-7}$ S/m usually show the largest ER effect because, in this case, the strength of interfacial polarization can reach a maximum.

The microstructural change of the ERF was directly observed with an optical microscope with a dc high-voltage source. When the electric field was not applied, the PANI/bentonite nanohybrids particles were found to be randomly dispersed in silicone oil like a so-called Newtonian fluid. However, when an electric field was applied, the particles started to form fibrillated chain structures along the direction of the electric field (as shown in Figure 7). With and without the electric field, the difference in the liquid-to-solid transition led to a change in the rheological properties.[39–42] The shear stress of the ERFs made of PANI/bentonite nanohybrids (20 wt % in silicone oil, controlled shear rate (CSR) mode) as a function of the shear rate is shown in Figure 8 under external electric fields. In the absence of a dc electric field, the ERF behaved like a Newtonian fluid, with a shear stress that increased linearly with shear rate. When a dc electric field was applied, the PANI/bentonite nanohybrids ERF showed typical Bingham fluid behavior, which was a typical rheological characteristic of an ERF.[42–47] The large dynamic yield stress, obtained approximately as the plateau stress at low shear rate, indicated that the suspension was strongly solidified by an applied electric field. It is known that the rheological behavior of an ER suspension is the result of organization and field-induced assembly into fiberlike structures. This structural change was mainly dominated by the electric-field-induced electrostatic interaction and the shear-field-induced hydrodynamic forces. The large polarizability of the ER particles was important in producing a strong and fast electrostatic interaction that could maintain the fibrous structures and, thus, keep the rheological properties stable under shear flow.

## CONCLUSIONS

In summary, a modified interfacial polymerization was used to prepare a series of PANI/bentonite nanohybrids. We found that the concentration of bentonite and surfactant in the synthetic route played a critical role in controlling their structure, morphology, and optical properties. The XRD results showed that PANI could be intercalated into the interlayer of bentonite. The

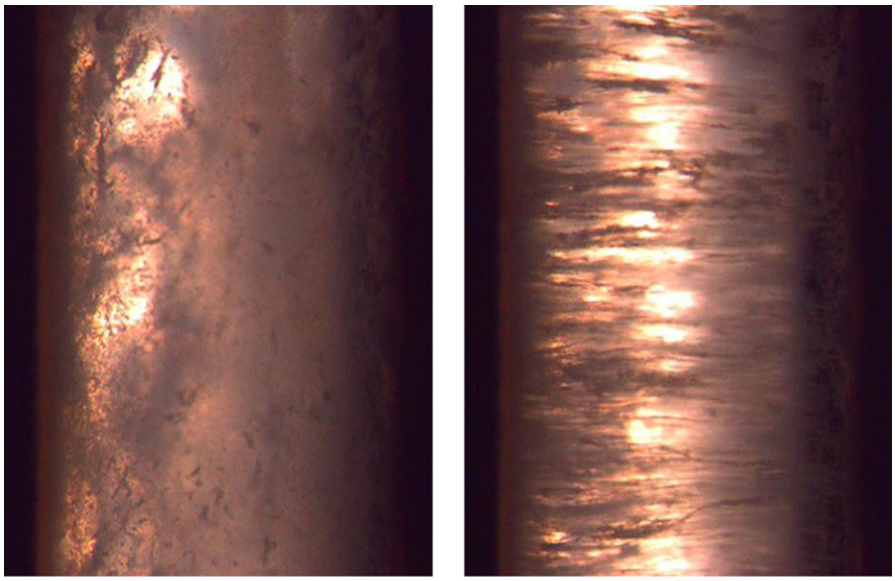


**Figure 7.** Optical microscopic images of the PANI/bentonite nanocomposite based ERF (a) without an electric field and (b) with an electric field. [Color figure can be viewed in the online issue, which is available at wileyonlinelibrary.com.]

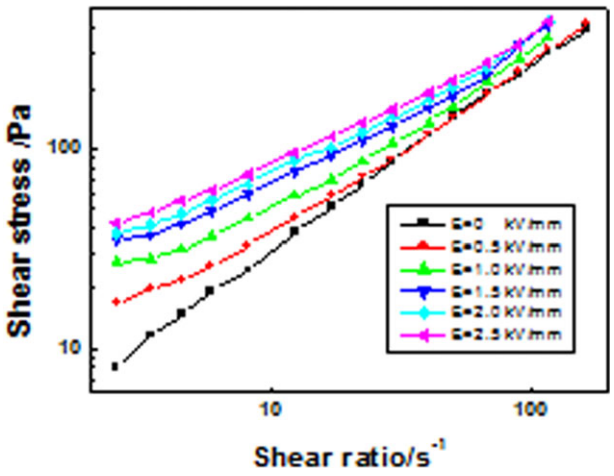


**Figure 8.** Flow curves (shear stress vs shear rate) of the PANI/bentonite nanocomposite based ERFs (20 wt % particle concentration) under various electric field strengths. [Color figure can be viewed in the online issue, which is available at wileyonlinelibrary.com.]

interlayer space was increased from 1.25 to 1.486 nm. CTAB was used to modify the surface of bentonite and was helpful in hybridizing with PANI for its hydrophobic properties. It is interesting that both the intercalation and coating structure could be found in the PANI/bentonite nanohybrid. TEM and SEM images verified that the surface of the bentonite plate was coated by the PANI nanofiber. This general facile synthetic method could make PANI nanofibers a material application platform for systematic studies of conducting polymer nanostructures, such as ERFs.

## ACKNOWLEDGMENTS

The authors gratefully acknowledge financial support from the National Natural Science Foundation of China (contract grant number NSFC 51072087), the Project Sponsored by the Scientific Research Foundation for the Returned Overseas Chinese Scholars, State Education Ministry, the Opening Project of State Key Laboratory of Polymer Materials Engineering (Sichuan University)(contract grant number KF201303), and Shandong Distinguished Middle-Aged and Young Scientist Encourage and Reward Foundation (contract grant number BS2011CL016).

## REFERENCES

1. MacDiarmid, A. G.; Jones, W. E.; Norris, I. D.; Gao, J.; Johnson, A. T.; Pinto, N. J.; Hone, J.; Han, B.; Ko, F. K.; Okuzaki, H.; Llaguno, M. *Synth. Met.* **2001**, *119*, 27.
2. Zujovic, Z. D.; Wang, Y.; Bowmaker, G. A.; Kaner, R. B. *Macromolecules* **2011**, *44*, 2735.
3. Baker, C. O.; Shedd, B.; Innis, P. C.; Whitten, P. G.; Spinks, G. M.; Wallace, G. G.; Kaner, R. B. *Adv. Mater.* **2008**, *20*, 155.
4. Liu, Z.; Zhang, X.; Poyraz, S.; Surwade, S. P.; Manohar, S. K. *J. Am. Chem. Soc.* **2010**, *132*, 13158.
5. Stejskal, J.; Sapurina, I.; Trchova, M. *Prog. Polym. Sci.* **2010**, *35*, 1420.
6. Tran, H. D.; Wang, Y.; Darcy, J. M.; Kaner, R. B. *Am. Chem. Soc. Nano.* **2008**, *2*, 1841.
7. Guo, S.; Dong, S.; Wang, E. *Small* **2009**, *5*, 1869.
8. Wei, Z. X.; Zhang, Z. M.; Wan, M. X. *Langmuir* **2002**, *18*, 917.
9. Zhang, Z. M.; Wan, M. X.; Wei, Y. *Adv. Funct. Mater.* **2006**, *16*, 1100.
10. Li, D.; Huang, J. X.; Kaner, R. B. *Acc. Chem. Res.* **2009**, *42*, 135.
11. Li, D.; Xia, Y. N. *Nat. Mater.* **2004**, *3*, 753.
12. Aleshin, A. N. *Adv. Mater.* **2006**, *18*, 17.
13. Kim, D.; Kim, E.; Lee, J.; Hong, S.; Sung, W.; Lim, N.; Park, C. G.; Kim, K. *J. Am. Chem. Soc.* **2010**, *132*, 9908.
14. Han, J.; Wang, L.; Guo, R. *Macromol. Rapid Commun.* **2011**, *32*, 729.
15. Guo, Z.; Ruegger, H.; Kissner, R.; Ishikawa, T.; Willeke, M.; Walde, P. *Langmuir* **2009**, *25*, 11390.
16. Li, G. C.; Li, Y. M.; Li, Y.; Peng, H. R.; Chen, K. Z. *Macromolecules* **2011**, *44*, 9319.
17. Yang, G.; Hou, W. H.; Feng, X. M.; Xu, L.; Liu, Y. G.; Wang, G.; Ding, W. P. *Adv. Funct. Mater.* **2007**, *17*, 401.
18. Giannelis, E. P. *Adv. Mater.* **1996**, *8*, 29.
19. Bourlinos, A. B.; Chowdhury, S. R.; Jiang, D. D.; An, Y. U.; Zhang, Q.; Archer, L. A.; Giannelis, E. P. *Small* **2005**, *1*, 80.
20. Xi, Y.; Ding, Z.; He, H.; Frost, R. L. *J. Colloid Interface Sci.* **2004**, *277*, 116.
21. Xi, Y. F.; Frost, R. L.; He, H. P.; Kloprogge, J. T.; Bostrom, T. *Langmuir* **2005**, *21*, 8675.
22. Yoshimoto, S.; Ohashi, F.; Kanneyama, T. *Macromol. Rapid Commun.* **2004**, *25*, 1687.
23. Sudha, J. D.; Sasikala, T. S. *Polymer* **2007**, *48*, 338.
24. Halsay, T. C. *Science* **1992**, *258*, 761.
25. Block, H.; Kelly, J. P. *J. Phys. D: Appl. Phys.* **1988**, *21*, 1661.
26. Tao, R.; Sun, J. M. *Phys. Rev. Lett.* **1991**, *67*, 398.
27. Gamota, D.; Filisko, F. E. *J. Rheol.* **1991**, *35*, 399.
28. Parthasarathy, M.; Klingenberg, D. *J. Mater. Sci. Eng. R.* **1996**, *17*, 57.
29. Wen, W. J.; Huang, X. X.; Yang, S. H.; Lu, K. Q.; Sheng, P. *Nat. Mater.* **2003**, *2*, 727.
30. (a) Hong, C. H.; Choi, H. J.; Jhon, M. S. *Chem. Mater.* **2006**, *18*, 2771; (b) Jin, H. J.; Choi, H. J.; Yoon, S. H.; Myung, S. J.; Shim, S. E. *Chem. Mater.* **2005**, *17*, 4034.
31. Shen, R.; Wang, X. Z.; Lu, Y.; Wang, D.; Sun, G.; Cao, Z. X.; Lu, K. Q. *Adv. Mater.* **2009**, *21*, 4631.
32. (a) Cao, J. G.; Huang, J. P.; Zhou, L. W. *J. Phys. Chem. B.* **2006**, *110*, 11635; (b) Tan, P.; Tian, W. J.; Wu, X. F.; Huang, J. Y.; Zhou, L. W.; Huang, J. P. *J. Phys. Chem. B* **2009**, *113*, 9092.
33. Lengalova, A.; Pavlinek, V.; Saha, P.; Stejskal, J.; Kitano, T.; Quadrat, O. *Phys. A: Stat. Mech. Appl.* **2003**, *321*, 411.
34. (a) Espin, M. J.; Delgado, A. V.; Plocharski, J. *Langmuir* **2005**, *21*, 4896; (b) Ramos-Tejada, M. M.; Arroyo, F. J.; Delgado, A. V. *Langmuir* **2010**, *26*, 16833.

35. Lee, B. M.; Kim, J. E.; Fang, F. F.; Choi, H. J.; Feller, J.-F. *Macromol. Chem. Phys.* **2011**, *212*, 2300.

36. Fang, F. F.; Choi, H. J.; Joo, J. *J. Nanosci. Nanotechnol.* **2008**, *8*, 1559.

37. Wang, B. X.; Zhao, X. P. *J. Solid State Chem.* **2006**, *179*, 1067.

38. Block, H.; Kelly, J. P.; Qin, A.; Watson, T. *Langmuir* **1990**, *6*, 6.

39. Wen, W. J.; Huang, X. X.; Sheng, P. *Soft Matter* **2008**, *4*, 200.

40. Krzton-Maziopa, A.; Wycislik, H.; Plocharski, J. *J. Rheol.* **2005**, *49*, 1177.

41. Cheng, Y. C.; Liu, X. H.; Guo, J. J.; Liu, F. H.; Li, Z. X.; Xu, G. J.; Cui, P. *Nanotechnology* **2009**, *20*, 055604.

42. (a) Cheng, Q.; Pavlinek, V.; He, Y.; Li, C.; Saha, P. *Colloid Polym. Sci.* **2009**, *287*, 435; (b) Cheng, Q.; Pavlinek, V.; Lengalova, A.; Li, C. Z.; He, Y.; Saha, P. *Micropor. Mesopor. Mater.* **2006**, *93*, 263.

43. (a) Yin, J. B.; Xia, X.; Xiang, L. Q.; Zhao, X. P. *J. Mater. Chem.* **2010**, *20*, 7096; (b) Yin, J. B.; Zhao, X. P. *J. Phys. Chem. B* **2006**, *110*, 12916; (c) Yin, J. B.; Zhao, X. P.; Xiang, L. Q.; Xia, X.; Zhang, Z. S. *Soft Matter* **2009**, *5*, 4687.

44. (a) Wang, B. X.; Zhao, X. P. *Adv. Funct. Mater.* **2005**, *15*, 1815;(b) Wang, B. X.; Zhao, X. P. *Langmuir* **2005**, *21*, 6553.

45. (a) Wang, B. X.; Zhou, M.; Rozynek, Z.; Fossum, J. O. *J. Mater. Chem.* **2009**, *19*, 1816; (b) Wang, B. X.; Rozynek, Z.; Fossum, J. O.; Knudsen, K. D.; Yu, Y. D. *Nanotechnology* **2012**, *23*, 075706.

46. (a) Choi, H. J.; Jhon, M. S. *Soft Matter* **2009**, *5*, 1562; (b) Cho, M. S.; Choi, H. J.; To, K. W. *Macromol. Rapid Commun.* **1998**, *19*, 271.

47. Zhang, W. L.; Liu, Y. D.; Choi, H. J. *J. Mater. Chem.* **2011**, *21*, 6916.